Int. J. Solids Structures, 1971, Vol. 7, pp. 863 to 881. Pergamon Press. Printed in Great Britain

PLASTIC DEFORMATION AND PERFORATION OF THIN PLATES RESULTING FROM PROJECTILE IMPACT†

C. A. CALDER‡

Washington State University, Pullman, Washington

and

W. GOLDSMITH§

University of California, Berkeley, California

Abstract—The dynamic response of thin plates subjected to projectile impact was studied experimentally by measuring projectile velocity, permanent deformation, dynamic strain and displacements and by examining the growth of plastic deformation and motion of the projectile with a high speed framing camera. Most of the experimental work was performed with $\frac{1}{2}$ in. diameter steel projectiles, spherical or cylindro–conical in shape, centrally striking a 2024–0 aluminum plate, 0·050 in. thick and clamped on a $14\frac{1}{2}$ in. diameter, at normal velocities ranging from 75 to 933 ft/sec. Projectile speeds were chosen so as to produce significant plastic deformation at the lower velocities and complete perforation at the higher velocities. The circular boundary of the plastic zone was found to propagate away from the point of impact at about 8800 in./sec at all impact velocities. A simplified large deflection solution for the final central deflection of a rigid/plastic linearly work-hardening plate showed good agreement with the data and correlation between various perforation theories and experimental data was found to improve with increasing projectile velocity.

INTRODUCTION

THE general problem of the response of structures subjected to dynamic loading, and particularly to projectile impact loading, is very complex and analytical solutions are usually obtained only for very idealistic simplifications to the problem. When a projectile strikes a target both the projectile and target may deform elastically, plastically, break up, burn, or even explode depending on the level of impact velocity and such factors as projectile and target shapes, target thickness and mechanical properties of the projectile and target. At the present time no analytical representation involving all the factors cited above can be constructed. Consequently, an effective model incorporating the principal mechanisms involved in the region of interest is needed to make the analysis manageable.

† Based upon a dissertation submitted in partial fulfillment of the requirements of the Ph.D. degree. Work supported in part by the National Science Foundation.

‡ Assistant Professor, Department of Mechanical Engineering.

§ Professor, Division of Applied Mechanics.

The present paper is concerned with both theoretical and experimental investigations of the response of thin aluminum plates under projectile impact when either large scale deformations without perforation are produced or when perforation occurs well beyond the ballistic limit. This study represents an extension of previous work of similar nature involving elastic collisions and perforation at minimal velocities [1].

Considerable effort has been expended in theoretical studies on the dynamic response of thin circular plates composed of rigid/plastic or viscoplastic materials, either simply supported or clamped, when subjected to impulsive loading over either all or a portion of their surfaces [2–6], based solely upon bending effects. Comparison of the experimental data with such predictions indicates that the theory grossly overestimates the actual final plate deflection, but good correlation was obtained when membrane effects were also considered [7]. Analysis of the problem based solely upon membrane theory, such as Ref. [8], yields non-linear relations requiring either purely numerical solutions or additional simplifying hypotheses to linearize the equations.

In contrast to blast-loading, theoretical work covering projectile impact on plates is rather fragmentary. The elastic impact problem on both an infinite and a clamped circular plate was solved for an arbitrarily specified triangular-shaped forcing function concentrated at the origin [1]. Good qualitative agreement was noted between experimental impact data for the two types of boundary conditions and corresponding theoretical predictions.

An analysis for the impact of a rigid cylinder on a rigid/perfectly-plastic circular plate has been obtained for the somewhat unrealistic condition of constant projectile acceleration [9]. Another study of the transverse impact on such a plate involving a piecewise linear yield condition with a single yield hinge led to an acceptable solution only for the case of a constant transverse velocity input [10], where the velocity of propagation of the yield hinge was found to be proportional to the square root of the time after impact. A solution has also been developed for projectile impact on a clamped viscoplastic plate obeying the Mises yield condition that incorporates the dynamic interaction of the projectile and plate, the impact force or projectile motion not being specified *a priori* [11]. The inherent non-linearity in the problem was overcome by a linearization used previously in Ref. [6]. A method using these results to obtain the permanent deflection for the case of large deflections is given in Ref. [12]. An approximation to the solution of Ref. [11] gave good correlation with experimental data obtained from impact by 0·454 in. diameter cylindrical projectiles on $\frac{1}{4}$ in. thick mild steel plates, clamped on a 4 in. diameter, at velocities up to 1950 ft/sec [13].

Perforation phenomena introduces the additional complication of material fracture and have been analyzed only under a number of simplifying assumptions. One type of approach is based upon a momentum balance and prescribed deformations of the plate in the region of contact [14]. A quasi-analytical relation for the residual projectile velocity for a plug type perforation, assuming a prior knowledge of the minimum perforation velocity, has also been obtained by an energy balance. The solution was found to be in good agreement with experimental results at velocities up to 4000 ft/sec [15]. Perforation at minimal velocities up to 380 ft/sec of 0·050 in. thick, 2024-0 aluminum plates by $\frac{1}{4}$ and $\frac{1}{2}$ in. diameter cylindro–conical projectiles produced failure by petalling [1]. Predictions of various perforation theories were found to be in poor agreement with these experimental data. This was expected, as the assumptions used in these theories, such as constant projectile velocity and no deformation outside the region of projectile contact, were not even approximately satisfied.

ANALYTICAL CONSIDERATIONS

(a) *Plastic plate deformation under normal projectile impact*

By assuming a permanent deflection shape, it is possible to calculate the maximum central deflection due to normal projectile impact using an analysis for a perfectly-plastic plate developed by Duffey [16]. This simplified energy approach is extended here in an attempt to include work-hardening effects. The aluminum alloy (2024-0) used in most of the experimental work in this investigation is highly work-hardening and results have shown strain levels of over 2 per cent at a radius of 1·5 in. from the impact point. However, since the greatest deformation occurs inside this radius, strain levels on the order of 6–8 per cent or more are undoubtedly attained requiring an account for the large amount of work-hardening present. Assuming the usual thin plate, plane stress and symmetry conditions, then the total plastic strain energy E_p can be written as

$$E_p = \int_{\text{Vol}} \left(\int [\sigma_r \, \mathrm{d}\varepsilon_r + \sigma_\phi \, \mathrm{d}\varepsilon_\phi] \right) \mathrm{d}V \tag{1}$$

where σ and ε are stress and strain, and subscripts r, ϕ refer to the radial and circumferential directions, respectively. Utilizing the one-to-one correspondence between stress and strain characteristic of the deformation theory of plasticity, assuming $\varepsilon_\phi \cong 0$, neglecting the contribution of the second term in equation (1) and applying the Mises condition $\sigma_r^2 - \sigma_r\sigma_\phi + \sigma_\phi^2 = (\sigma_y + \alpha\varepsilon_r)^2$, where the flow stress σ_0 has been replaced by $(\sigma_y + \alpha\varepsilon_r)$ to approximately account for linear work hardening of the material, gives

$$E_p = \frac{4\pi h}{(1 - \nu + \nu^2)^{\frac{1}{2}}} \int_0^R (\sigma_y \varepsilon_r + \tfrac{1}{2}\alpha\varepsilon_r^2) r \, \mathrm{d}r. \tag{2}$$

In this expression, σ_y is the initial yield stress, α the linear work-hardening parameter, ν is Poisson's ratio and $2h$ and R are the plate thickness and radius, respectively. For the large deflections, the radial stretching strain for small radial displacements can be approximately written as

$$\varepsilon_r = \frac{1}{2}\left(\frac{\partial w}{\partial r}\right)^2 \tag{3}$$

where w is plate deflection and r the radial coordinate. Thus, equation (2) gives the approximate plastic work done as

$$E_p = \frac{4\pi h}{(1 - \nu + \nu^2)^{\frac{1}{2}}} \int_0^R \left(\frac{1}{2}\sigma_y \left(\frac{\partial w}{\partial r}\right)^2 + \frac{\alpha}{8}\left(\frac{\partial w}{\partial r}\right)^4 \right) r \, \mathrm{d}r. \tag{4}$$

If a permanent deflection profile $w(r) = w_0 f(r)$, is assumed, where w_0 is the permanent deflection at $r = 0$, and the loss of kinetic energy of the projectile $(\Delta KE)_{\text{proj}}$ is set equal to the plastic energy E_p, the result is

$$\left[\int_0^R (f_{,r})^4 r \, \mathrm{d}r\right] w_0^4 + \left[\frac{4\sigma_y}{\alpha}\int_0^R (f_{,r})^2 r \, \mathrm{d}r\right] w_0^2 - \frac{2(1 - \nu + \nu^2)^{\frac{1}{2}}}{\alpha\pi h}(\Delta KE)_{\text{proj}} = 0. \tag{5}$$

This equation can be solved for the permanent central deflection w_0 when the deformation profile is known or assumed.

In the present investigation, a good approximation for the permanent deformation profile of the plate subject to projectile impact was empirically found to be

$$w(r) = w_0 e^{-r} \tag{6}$$

where r is the radius in inches from the point of impact. In this case equation (5) becomes

$$w_0^4 + \left(\frac{16\sigma_y}{\alpha}\right) w_0^2 - \frac{32(1-v+v^2)^{\frac{1}{2}}}{\alpha\pi h}(\Delta KE)_{\text{proj}} = 0. \tag{7}$$

This result incorporates several major simplifying assumptions and does not pretend to be a rigorous solution to the physical problem. However, some of these assumptions have been checked by Duffey [16] against the results of a finite-difference type computer solution developed for the dynamic response of structures [17]. The contribution of plastic energy due to ε_ϕ was found to be less than 3 per cent of the initial kinetic energy and a term $\partial u/\partial r$ neglected in equation (3), where u is the radial displacement, was evaluated to be roughly 15 per cent of ε_r. As the plate deformation in the present work is considerably more localized, it is believed that these approximations will be improved.

(b) *Thin plate perforation*

Results of the present perforation experiments indicated that the primary mode of failure in the thin ductile plates occurred by petalling in the case of cylindro–conical projectiles and by a combination of dishing and plugging in the case of spheres. The terminal projectile velocity V_f, in terms of its initial value V_i, was predicted by Thomsen [18] to be

$$V_f^2 = V_i^2 - \frac{4\pi r_0^2 h}{m}\left[\frac{\sigma_0}{2} + \frac{\rho}{3}V_i^2\right]. \tag{8}$$

This is based upon a balance involving the change of kinetic energy of the projectile, of mass m, the static work of plastic deformation and the effects of transverse motion.

For a sphere, an analogous derivation involving plate shear yields [15]

$$V_f = \left[\frac{m}{m+m_p}\right](V_i^2 - V_x^2)^{\frac{1}{2}} \tag{9}$$

where V_x is the minimum perforation velocity or ballistic limit and m_p is the plug mass. For a cylindro–conical projectile, $m_p = 0$ so that equation (9) becomes

$$V_f = (V_i^2 - V_x^2)^{\frac{1}{2}}. \tag{10}$$

Use of a momentum balance with an assumed plate deformation pattern yields an expression for the terminal velocity of a cylindro–conical projectile with half cone angle θ given by [14]

$$V_f = \frac{m}{m + 2\pi\rho h r_0^2 \sin\theta} V_i. \tag{11}$$

EXPERIMENTAL APPARATUS AND PROCEDURE

The experimental arrangement of the present investigation is similar to that used previously for elastic impact and perforation of thin plates [1], but also featured a higher

velocity pneumatic gun capable of achieving velocities to 1500 ft/sec and a modern high speed framing camera. The Beckman and Whitley model WB-2 high speed framing camera records 79 frames of data on 35 mm film at continuously variable framing rates from less than 20,000 up to 1 million/sec. Illumination for the high speed camera was provided by a GE FT-524 (clear) or a GE FT-503 (frosted) xenon flash tube energized from a 100 μF capacitor bank charged at 3600 V. The xenon flash tube provides a peak light output of over 200 Mlm with a duration of 300–500 μsec and was used to produce a shadowgraph image.

The high speed framing camera can provide up to 79 data points of position–time for the projectile. The impact force produced by the contact process can be determined by evaluating the deceleration of the projectile, considered to be totally rigid, requiring two differentiations of the observed position–time relation for the projectile with all such inherent inaccuracies.

To overcome the drawbacks of the usual techniques of graphical or numerical differentiation of experimental data, a method was developed that fitted to the data an appropriate analytical function with a number of unknown parameters. The evaluation of these quantities permitted the determination of the velocity and deceleration by analytical differentiation [19].

The resistance strain gages employed to measure dynamic strains in the plate were BLH SR-4, types FAP-12-12 and FAB-12-12. The gages were mounted on the impact side of the plate to record the maximum (bending plus membrane) radial strains at positions $1\frac{1}{2}$ and 3 in. from the impact point. The gages were used in a potentiometer type circuit and calibrated dynamically by observing the voltage change on the oscilloscope caused by connecting and disconnecting shunt resistances (2000 to 10^6 Ω) in parallel with the strain gage through use of a 60 cycle oscillator. Four Bently† noncontacting inductance type displacement sensors, located on the distal side of the plate (Fig. 1), simultaneously measured the transverse motion of the plate at radii of 2, 3, 4 and 5 in. from the point of impact. These were statically calibrated by noting the signal change at various distances from the target produced by the motion of micrometer heads. Perforation or rebound velocities of the projectile were determined by an inductance type of velocity gage consisting of two coils as reported in Ref. [20].

Two Tektronix 565 dual beam oscilloscopes, equipped with type 3A1 amplifiers and attached cameras, recorded the signals from the strain, displacement and velocity gages using a chopping mode operating at a frequency of 200 kHz. One scope also provided a delayed signal for triggering the flash tube.

Except for several selected tests on 4×4 ft freely-suspended plates 0·050 in. thick, all impacts were performed at the center of $15\frac{1}{2}$ in. diameter circular plates clamped in a circular frame on a $14\frac{1}{4}$ in. diameter by 12 machine bolts (Fig. 1). Windows were provided in the frame to permit the high speed camera to view the plate profile during impact. The windows leave the two short sections of the plate boundary unclamped but this did not noticeably affect the symmetry of the data, principally because plastic deformation never reached the plate boundary. The target materials consisted of either 2024-0 or 1100-H14 aluminum sheets, 0·050 in. thick, or of 18 gage cold rolled steel plates.

The deformation tests were conducted with $\frac{1}{2}$ in. diameter chrome alloy steel spheres and the perforation tests with either $\frac{1}{2}$ in. diameter steel spheres or $\frac{1}{2}$ in. diameter cylindro–

† Manufactured by Bently Corporation, Minden, Nevada.

conical steel (drill rod) projectiles with a 60° cone angle and 0·75 in. long. Selected runs were also made with $\frac{1}{4}$ in. diameter steel spheres and $\frac{1}{4}$ in. diameter cylindro–conical steel (drill rod) projectiles.

A quasi-static run was performed in a Tinius Olsen testing machine. A $\frac{1}{2}$ in. diameter sphere in contact with the plate center was loaded and the load vs. center deflection recorded. At various intervals, the plate was unloaded and the permanent deformation at a number of positions measured by means of a profilometer [19]. The plate was then reloaded and the procedure repeated until failure (fracture) of the plate occurred.

EXPERIMENTAL RESULTS

(a) *Plate deformation without perforation*

A summary of the runs for the case of plate impact by a spherical projectile without perforation, involving a maximum velocity of 398 ft/sec for aluminum targets is presented

TABLE 1. SUMMARY OF PLATE DEFORMATION RUNS

Run	Projectile†	Plate‡	V_i (ft/sec)	V_f (ft/sec)	Permanent central deflection (in.)
AC-1	*a*	AC_1	106		0·174
AC-2	*a*	AC_1	199		0·321
AC-3	*a*	AC_1	303		0·522
AC-4	*a*	AC_1	398		0·675
AC-5	*a*	AC_1	397		0·655
AC-6	*a*	AC_1	Static		Fracture
AC-7	*b*	AC_1	549		0·329
AC-8	*c*	AC_1	172		Partial perforation
AC-9	*a*	AC_2	303		0·525
AC-10	*a*	AC_2	205		0·327
AI-1	*a*	*AI*	219		0·353
AI-2	*a*	*AI*	309		0·494
AI-3	*a*	*AI*	396		0·645
SC-1	*a*	*SC*	307		0·218
SC-2	*a*	*SC*	~400		0·305
SC-3	*a*	*SC*	493		0·394
SC-4	*a*	*SC*	80		0·030
SC-5	*a*	*SC*	204		0·141
Reb. 1	*a*	AC_1	75	− 6·7	–
Reb. 2	*a*	AC_1	110	− 3·7	0·212
Reb. 3	*a*	AC_1	176	−14·6	0·265
Reb. 4	*a*	AC_1	199	− 5·0	0·313
Reb. 5	*a*	AC_1	200	− 6·4	0·340
Reb. 6	*a*	AC_1	246	−13·3	0·404
Reb. 7	*a*	AC_1	301	− 6·5	0·523
Reb. 8	*a*	AC_1	350	−15·3	0·581
Reb. 9	*a*	AC_1	398	− 8·6	0·686

† *a*—$\frac{1}{2}$ in. diameter steel sphere, $m = 4{\cdot}78 \times 10^{-5}$ lb sec^2/in. *b*—$\frac{1}{4}$ in. diameter steel sphere, $m = 0{\cdot}60 \times 10^{-5}$ lb sec^2/in. *c*—$\frac{1}{2}$ in. diameter cylindro–conical steel projectile, 60° cone angle, 0·75 in. long, $m = 6{\cdot}66 \times 10^{-5}$ lb sec^2/in.

‡ AC_1—2024-0 aluminum, $14\frac{1}{4}$ in. diameter by 0·050 in. thick, clamped edge. AC_2—1100-H14 aluminum, $14\frac{1}{4}$ in. diameter by 0·050 in. thick, clamped edge. *AI*—2024-0 aluminum, 4 ft × 4 ft by 0·050 in. thick, freely suspended. *SC*—cold rolled steel plate, $14\frac{1}{4}$ in. diameter by 0·048 in. thick (18 ga.), clamped edge.

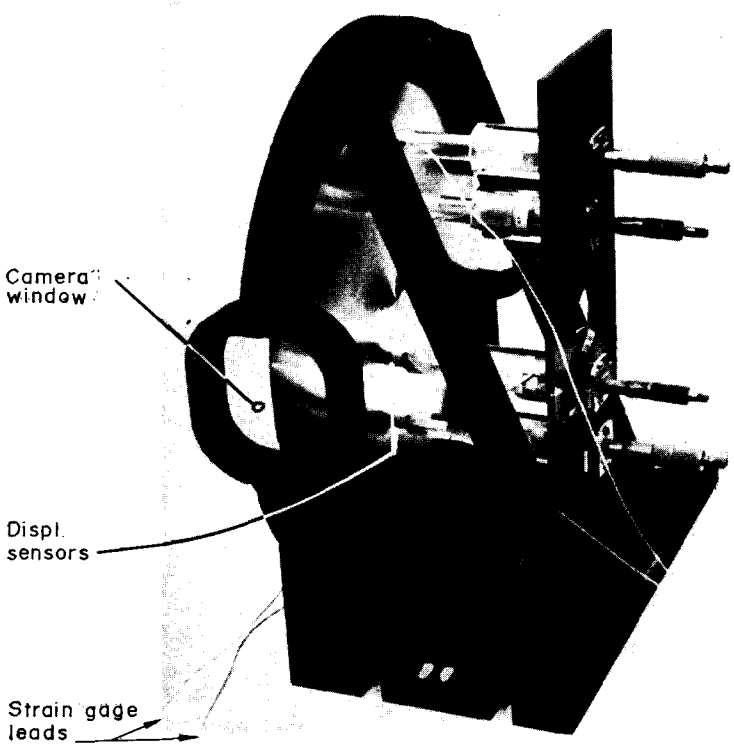

FIG. 1. Circular plate mount with attached displacement gages.

facing pp. 868

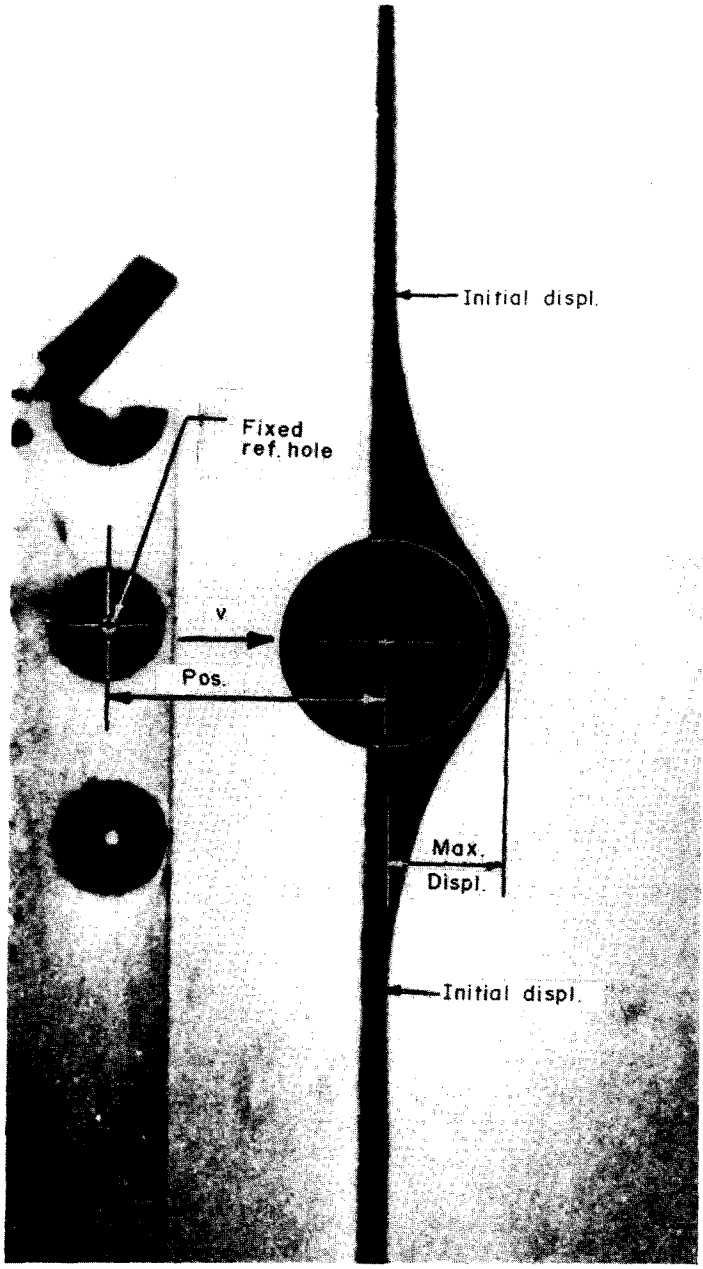

FIG. 2. Enlargement of individual frame illustrating the dynamic plate profile, projectile position measurement from fixed reference, and location of circles of initial displacement. Run *SC*-3, 63 μsec after impact by $\frac{1}{2}$ in. diameter steel sphere, V_i = 493 ft/sec.

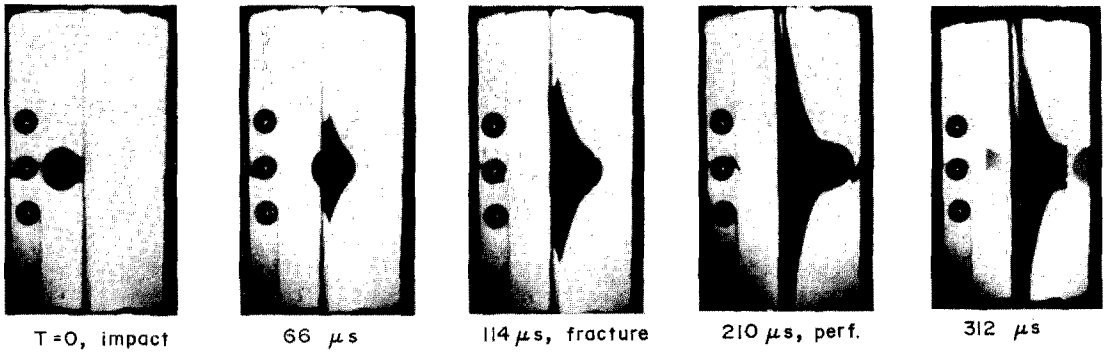

FIG. 12. Selected frames from perforation of clamped 2024–0 aluminum plates by a $\frac{1}{2}$ in. diameter sphere; 168,000 frames/sec, $V_i = 494$ ft/sec, $V_f = 315$ ft/sec.

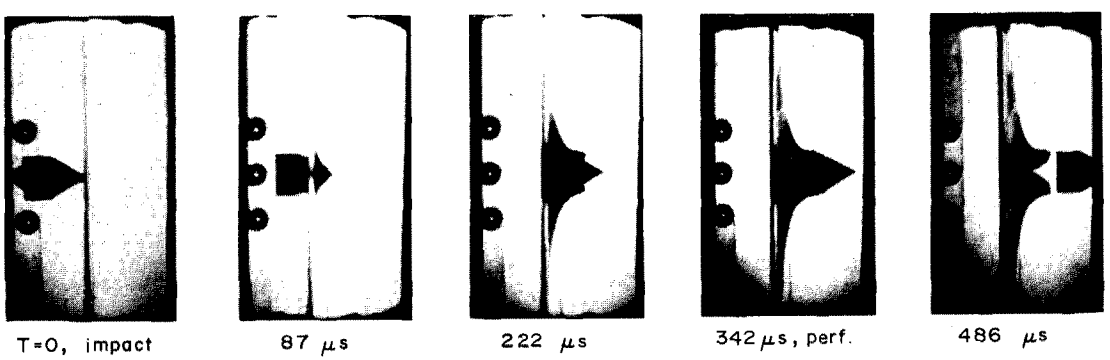

FIG. 13. Selected frames from perforation of a clamped 2024–0 aluminum plate by a $\frac{1}{2}$ in. diameter cylindro–conical projectile; 111,000 frames/sec, $V_i = 300$ ft/sec, $V_f = 195$ ft/sec.

Run PC-2:

$\frac{1}{2}$" dia. spherical steel proj.
V_i = 682 ft/sec
V_f = 587 ft/sec

Run PC-1:

$\frac{1}{2}$" dia. cylindro-conical steel proj.
V_i = 497 ft/sec
V_f = 445 ft/sec
(four petals)

Run PC-5:

$\frac{1}{2}$" dia. cylindro-conical steel proj.
V_i = 301 ft/sec
V_f = 195 ft/sec
(six petals)

FIG. 17. Perforation patterns for various cases; 2024-0 clamped circular plate, 14¼ in. diameter × 0·050 in. thick.

in Table 1. At $V_i = 450$ ft/sec the projectile perforated the aluminum plates. The rebound velocity was monitored only in a limited number of cases. The kinetic energy of the projectile rebound was found to be less than 1 per cent of the initial value and can thus be neglected in an energy balance. No permanent deformation of projectiles was observed in any of the tests of the present investigation.

An enlargement of a typical frame from run *SC*-3, shown in Fig. 2, illustrates the measurement of the projectile position from the fixed reference hole and also the dynamic plate profile and location of the circle of initial displacement. The radial strain histories at $1\frac{1}{2}$ and 3 in. from the impact point are presented in Fig. 3 for initial velocities of 199, 303 and 398 ft/sec. The peak strain for $V_i = 398$ ft/sec was not obtained due to gage failure at just over 2 per cent strain. The propagation velocity of the peak strain for runs *AC*-2 and *AC*-3 has a value of about 8800 in./sec. The radial strain history at $1\frac{1}{2}$ in. under conditions of partial perforation by the $\frac{1}{2}$ in. diameter cylindro–conical projectile is also given for comparison, run *AC*-8. Figure 4 shows the typical displacement histories obtained from the Bently gages positioned at 2, 3, 4 and 5 in. from the point of impact. The 3 in. displacement curve repeatedly shows a dip at about 1300 μsec attributed to elastic vibrations and the 5 in. curve peaks out at about the same time.

Permanent deflection results at positions 0, $\frac{1}{2}$ and 1 in. from the point of impact are plotted against impact velocity in Fig. 5, covering the full range of the gun. Permanent

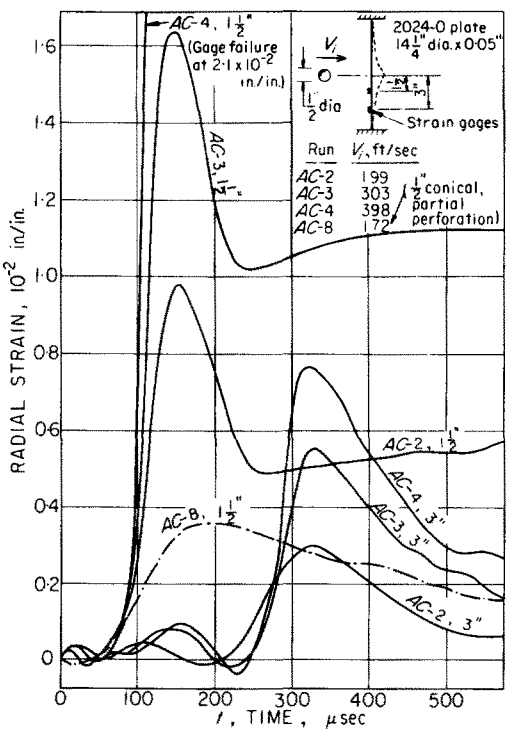

FIG. 3. Radial strain histories at $1\frac{1}{2}$ and 3 in. from the impact point for plate impact by $\frac{1}{2}$ in. diameter steel spheres.

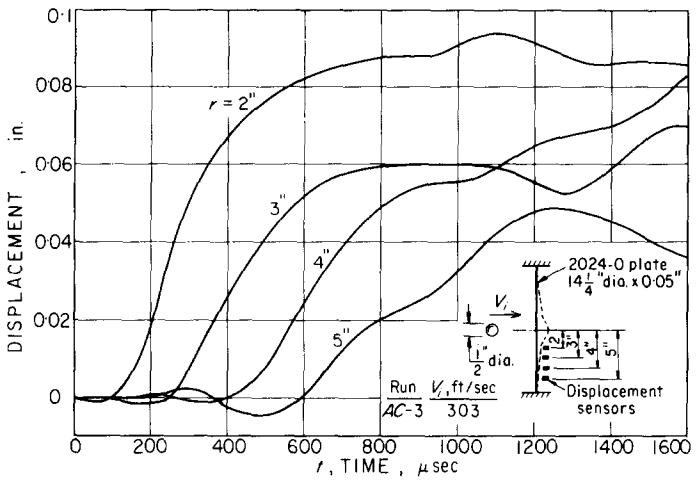

FIG. 4. Displacement history at 2, 3, 4 and 5 in. stations for impact by a $\frac{1}{2}$ in. diameter steel sphere, run *AC*-3.

deflections at the indicated radii increase almost linearly with impact velocity up to perforation at about 400 ft/sec where a sudden decrease occurs. Above this threshold the permanent deflection decreases monotonously with impact velocity. Figure 6 compares normalized deflection profiles w/w_0 with the empirical relation $w/w_0 = e^{-r}$ for 2024-0 plates, where w_0 is the permanent central deflection, with excellent correspondence indicated except in the region of projectile contact. The quasi-static deflection profile of run *AC*-6 occurring after unloading from a 700 lb central load is also included. The effect of the plate materials, boundary conditions and size of the striking sphere on the permanent deformation is shown in Fig. 7, where, as in the sequel, the deflection scale is substantially expanded. For 2024-0, the profile for the $14\frac{1}{4}$ in. diameter clamped plate is seen to be

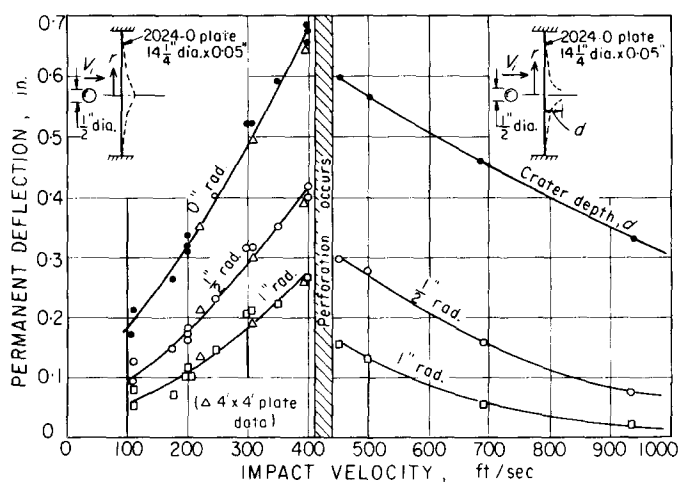

FIG. 5. Summary of permanent deflection over entire range of impact velocities for a $\frac{1}{2}$ in. diameter spherical steel projectile.

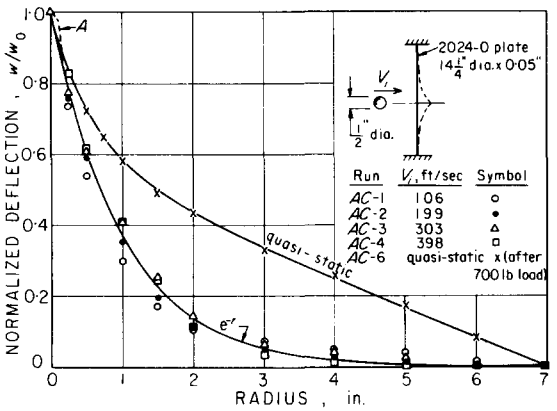

FIG. 6. Normalized permanent deflection profiles (with e^{-r} comparison curve) for plate impact by a $\frac{1}{2}$ in. diameter steel sphere at various impact velocities. Symbol A represents approximate profile linear center due to projectile shape.

identical to that for the 4×4 ft plate. The permanent deflection for 1100-H14 and mild steel is successively more concentrated around the impact point. Impact by a $\frac{1}{4}$ in. diameter sphere on a 2024-0 plate yields still further localization of the permanent deformation.

Plate profiles obtained from the framing camera at subsequent times after impact are shown in Fig. 8 for run *AC*-2. The dashed line is the statically measured final plate profile and indicates an elastic recovery from the maximum deflection profile. Figure 9 portrays similar results for twice the impact velocity, $V_i = 397$ ft/sec. Figures 8 and 9 both indicate the outward propagation of the first visible displacement of the plate, hereafter called a hinge, limited here to a distance of 2 in. from the center by the size of the viewing port. A plot of the location of this hinge with time for run *AC*-2, obtained from camera frame profiles as in Fig. 8, is given in Fig. 10. The curve has been extended out to 5 in. from displacement gage data similar to Fig. 4 using the arrival time of the initiation of gross displacement. The prediction of Ref. [10], fitted at $r = 5$ in., is included for com-

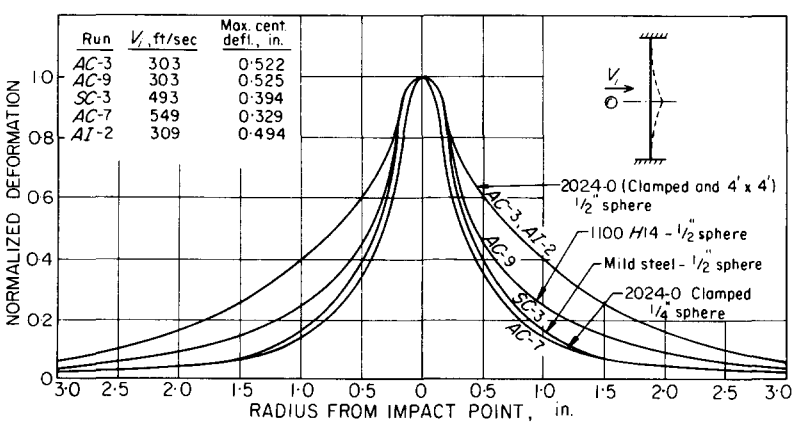

FIG. 7. Normalized permanent deformation profiles for the various plate materials used; impact by $\frac{1}{2}$ and $\frac{1}{4}$ in. diameter steel spheres.

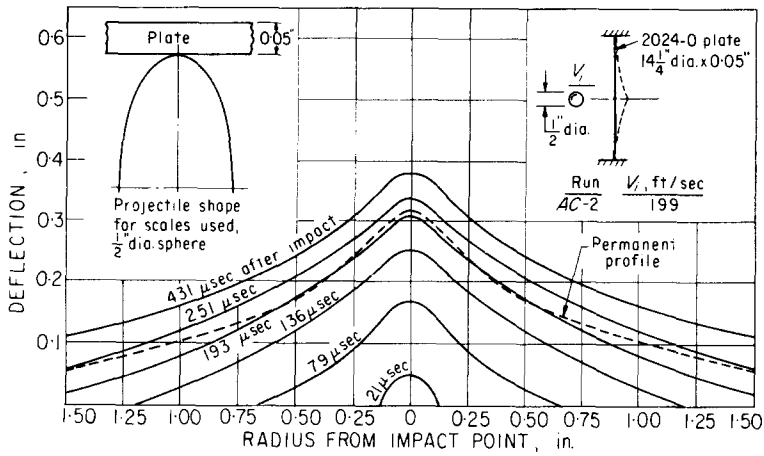

FIG. 8. Dynamic plate profiles at various times after impact by a $\frac{1}{2}$ in. diameter steel sphere, run *AC*-2.

parison as the only transient analytical solution available. The projectile position, velocity and force–time relations, evaluated by the least-mean-square procedure presented in Ref. [19] using an assumed force–time relation of $F(t) = At^2e^{-Bt}$, are given in Fig. 11 for run *AC*-2.

(b) *Plate perforation*

Table 2 provides a summary of the perforation runs with plate plug data from the first three tests, all conducted on clamped $14\frac{1}{4}$ in. diameter × 0·050 in. plates of 2024-0 aluminum alloy and the spherical and cylindro–conical projectiles previously described. Figure 12 shows selected frames from the perforation process by a $\frac{1}{2}$ in. diameter sphere. The plug or cap is formed in the third photograph and separates from the projectile in the next picture. The fourth photograph shows complete perforation, defined as the instant

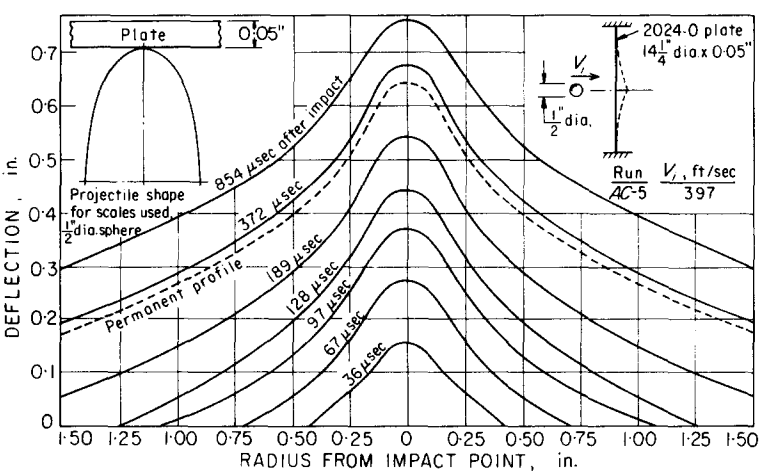

FIG. 9. Dynamic plate profiles at various times after impact by a $\frac{1}{2}$ in. diameter steel sphere, run *AC*-5.

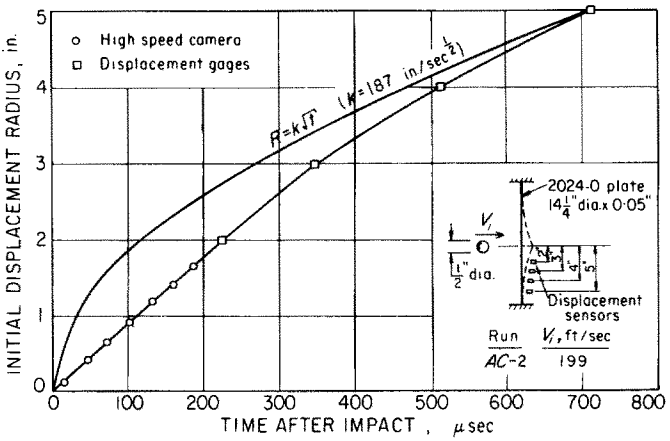

FIG. 10. Propagation of first visible displacement to a radius of 5 in.

when the contact of the projectile produces no further increase in the size of the target hole. A similar sequence is shown in Fig. 13.

The strain records at $1\frac{1}{2}$ and 3 in. for perforation by a $\frac{1}{2}$ in. diameter sphere and a $\frac{1}{2}$ in. diameter cylindro–conical projectile are shown in Figs. 14 and 15, respectively. The propagation velocity of the peak strain in both cases is about 8800 in./sec, the same as for plastic impact. The transient displacement records, similar to those shown in Fig. 4, for a perforation run with a $\frac{1}{2}$ in. spherical projectile (run *PC*-2) are presented in Fig. 16.

The plug or cap produced by spherical projectiles and the petals produced by cylindro–conical projectiles are illustrated in Fig. 17. Except at minimal perforation velocities, the number of petals formed is four. In run *PC*-5 a perforation with six petals occurred as shown in the third photograph of Fig. 17.

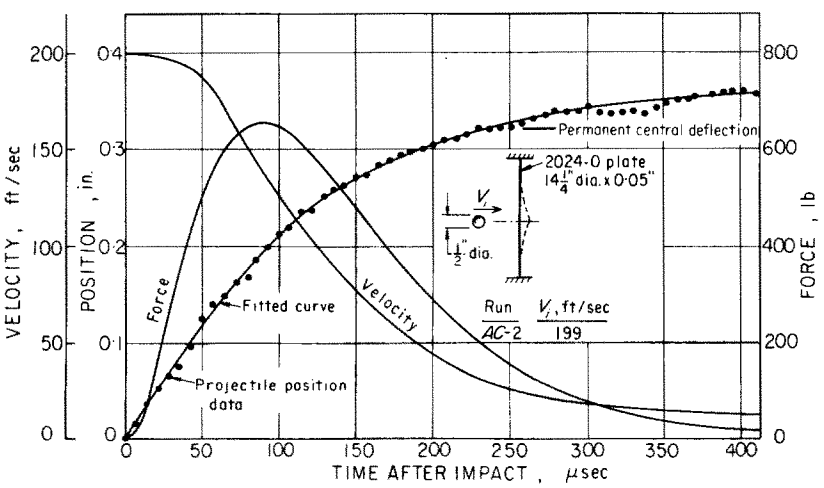

FIG. 11. Projectile position data with fitted curve and resulting velocity and force histories for impact by a $\frac{1}{2}$ in. diameter steel sphere: 139,000 frames/sec, run *AC*-2. Assumed force–time relation: $F(t) = At^2e^{-Bt}$.

TABLE 2. SUMMARY OF PLATE PERFORATION RUNS

Run	Projectile†	Plate‡	V_i (ft/sec)	V_f (ft/sec)	No. petals	Plate plug (cap) measurements: Mass (g)	Diameter (in.)	$2h$ (in.)	d (in.)
PC-1	*a*	AC_1	497	315		0·135	0·326	0·0413	0·093
PC-2	*a*	AC_1	682	587		0·187	0·378	0·0425	0·110
PC-3	*a*	AC_1	933	864		0·269	0·425	0·0427	0·145
PC-4	*b*	AC_1	1289	1016					
PC-5	*c*	AC_1	301	195	6				
PC-6	*c*	AC_1	391	302§	4				
PC-7	*c*	AC_1	497	445	4				
PC-8	*c*	AC_1	570	521	4				
PC-9	*c*	AC_1	840	803	4				
PC-10	*d*	AC_1	861	806	4				

† *a*—$\frac{1}{2}$ in. diameter steel sphere, $m = 4{\cdot}78 \times 10^{-5}$ lb sec^2/in. *b*—$\frac{1}{4}$ in. diameter steel sphere, $m = 0{\cdot}60 \times 10^{-5}$ lb sec^2/in. *c*—$\frac{1}{2}$ in. diameter cylindro–conical steel projectile, 60° cone angle, 0·75 in. long, $m = 6{\cdot}66 \times 10^{-5}$ lb sec^2/in. *d*—$\frac{1}{4}$ in. diameter cylindro–conical steel projectile, 60° cone angle, 0·625 in. long, $m = 1{\cdot}74 \times 10^{-5}$ lb sec^2/in.

‡ AC_1—2024-0 aluminum, $14\frac{1}{4}$ in. diameter by 0·050 in. thick, clamped edge.

§ Final velocity evaluated from high speed camera.

Transient plate profiles at the various stages of impact and perforation are shown in Fig. 18 for run *PC*-1. The dashed line represents the permanent deflection profile of the plate. At 113 μsec from impact the cap or plug has separated from the plate, the formation of the cap being initiated at 97 μsec.

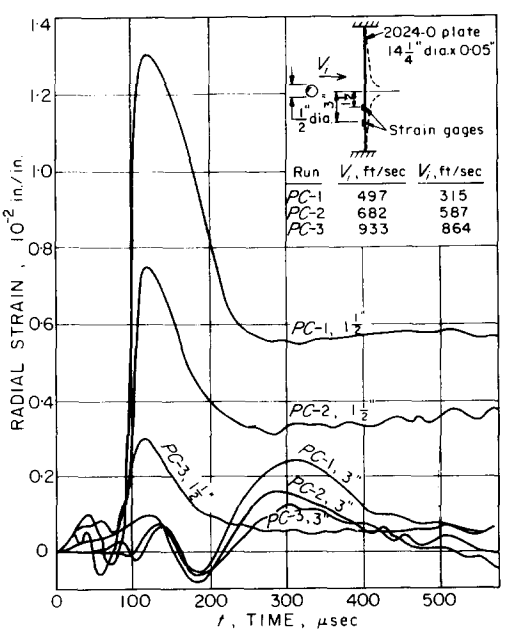

FIG. 14. Radial strain histories at $1\frac{1}{2}$ and 3 in. from the impact point for plates perforated by $\frac{1}{2}$ in. diameter spherical steel projectiles.

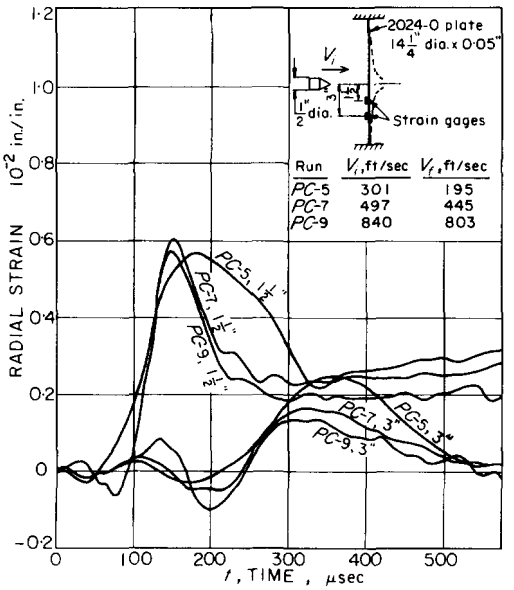

FIG. 15. Radial strain histories at $1\frac{1}{2}$ and 3 in. from the impact point for plates perforated by $\frac{1}{2}$ in. diameter cylindro–conical projectiles.

Figure 19 portrays the projectile position, velocity and force–time curves evaluated by the least-mean-square fit to camera data obtained during a typical perforation run involving a $\frac{1}{2}$ in. diameter sphere. Corresponding results from the perforation by a $\frac{1}{2}$ in. diameter cylindro–conical projectile are given in Fig. 20. In both cases, the assumed force–time relation was taken to be $F(t) = Ae^{-Bt}\sin^2 t$. The peak force developed in these two runs was about 1500 lb and about 540 lb, respectively. These compare to a value of 1500 lb for the static removal of a $\frac{1}{2}$ in. diameter plug in a material with a shear strength of 19,000 psi, representative of 2024-0 aluminum.

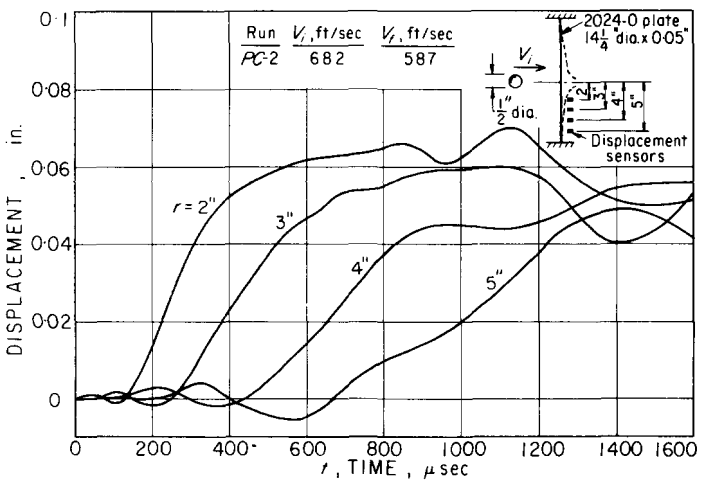

FIG. 16. Displacement history at 2, 3, 4 and 5 in. stations for perforation by a $\frac{1}{2}$ in. diameter steel sphere, run *PC*-2.

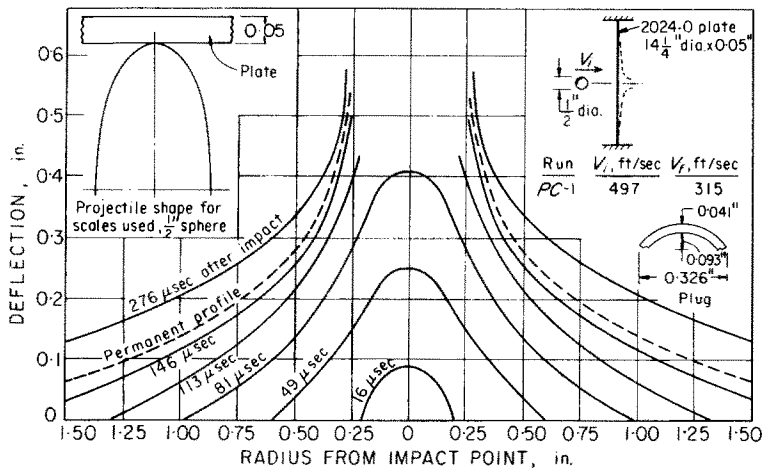

FIG. 18. Plate profiles at various times after impact for perforation by a $\frac{1}{2}$ in. diameter steel sphere, run *PC*-1.

DISCUSSION

Plastic impact

The strain records in Fig. 3 from stations on the impact side exhibit a large amount of attenuation and dispersion with a fast tensile rise to a peak value and then a reduction to a plateau which is approximately the permanent radial strain at that location. As both membrane and radial bending strains are tensile on the impact side, the gages provide a record of the absolute maximum strains reached at the $1\frac{1}{2}$ and 3 in. locations. The early elastic motion occurring before arrival of the principal transient is similar in nature

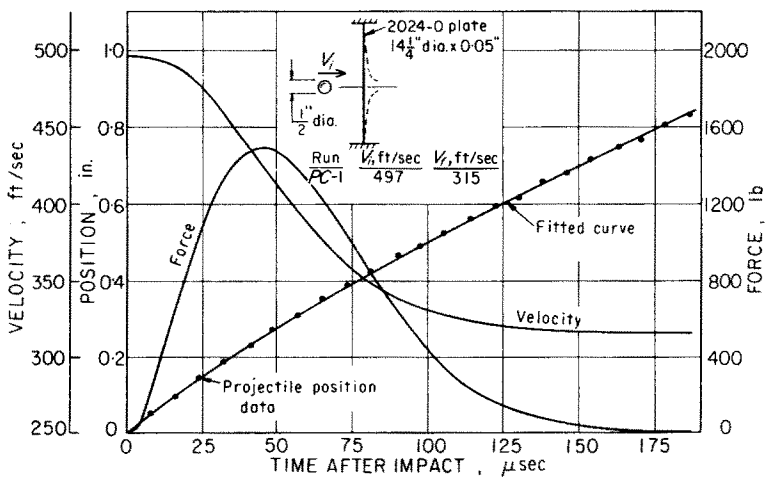

FIG. 19. Projectile position data with fitted curve and resulting velocity and force histories for perforation by a $\frac{1}{2}$ in. diameter steel sphere; 123,000 frames/sec, run *PC*-1. Assumed force–time relation: $F(t) = Ae^{-Bt}\sin^2 t$.

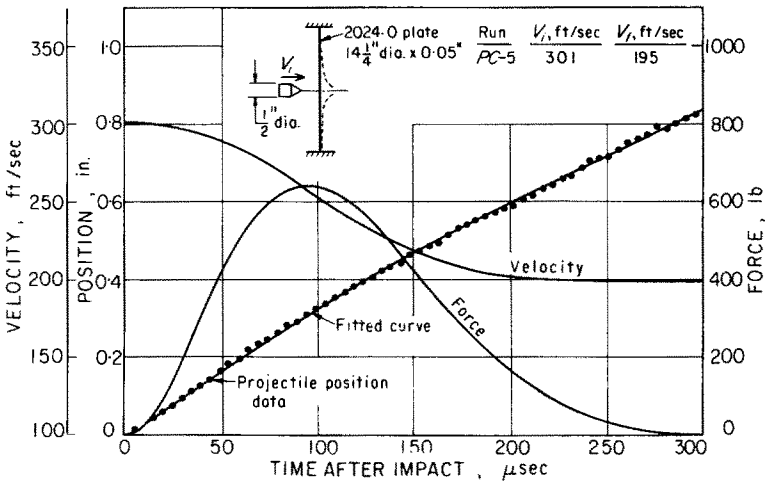

FIG. 20. Projectile position data with fitted curve and resulting velocity and force histories for perforation by a $\frac{1}{2}$ in. diameter cylindro–conical projectile; 203,000 frames/sec, run *PC-5*. Assumed force–time relation: $F(t) = Ae^{-Bt}\sin^2 t$.

to the entire strain history observed in purely elastic impact [1]. The amplitudes of both of these elastic disturbances is one order of magnitude smaller than the peak plastic strain. The average propagation velocity of the strain peaks between the $1\frac{1}{2}$ and 3 in. stations of 8800 in./sec is more than an order of magnitude slower than that of elastic waves in such plates. Although the amplitudes are an order of magnitude larger, the shapes of the displacement records shown in Fig. 4 are quite similar to those given in Ref. [1]. In both cases small amplitude displacements of the plate were observed before initiation of the large motion in the direction of impact.

The high degree of work-hardening and ductility of 2024-0 aluminum facilitate the absorption of energy over a greater region relative to the other materials, as illustrated in Fig. 7. However, when the impact velocity is sufficiently high, the energy cannot be dissipated fast enough through the spreading of plastic deformation and fracture of a plug occurs. The 1100-H14 aluminum plate cannot absorb as much energy without perforation as the 2024-0 plate because it is less ductile and does not work-harden, even though the yield stress of 1100-H14 of about 17,000 psi is significantly greater than the value of about 12,000 psi for 2024-0 aluminum. The almost identical terminal profiles of the 2024-0 clamped and freely suspended plates indicate that the plastic deformation never propagates out to the clamped boundary and that reflection of faster elastic waves to the plastic boundary have little or no effect. In the present tests, plastic deformation did not propagate to the plate boundary. However, other experimental investigations have shown wide-spread plastic deformation in the target [13, 21–23].

The results for the hinge position shown in Fig. 10 indicate a nearly constant velocity of propagation of 8800 in./sec out to a radius of 3 in. with a subsequent progressive reduction to a value of about 4700 in./sec at $r = 5$ in. These data are in quantitative disagreement with the predictions of Ref. [10], matched at the outmost observations station; this is undoubtedly due to the experimental deviations from the point impact conditions and ideal material behavior hypothesized. Using high speed photography, Munday and

Newitt [23] measured the propagation velocity of a plastic hinge in studies on blast loaded copper disks of 4 in. diameter and 0·002 in. thick, and also found a faster hinge propagation near the center. In this case, the plastic hinge formed at the clamped edge and propagated inward to the plate center with a velocity varying from 300 in./sec near the edge to about 7000 in./sec at the center. The evaluation of projectile position, velocity and force entails the mathematical fitting to the high speed camera data of a doubly integrated assumed force function selected by considering the physical conditions of the problem and the available experimental and theoretical results. The assumed force relation stipulated for this case, $F(t) = At^2e^{-Bt}$, leads to a position–time equation that, considering experimental scatter, is in excellent accord with the camera data as shown in Fig. 11. The above expression is similar to that found experimentally for elastic impacts but differs significantly from results for the minimal perforation condition of Ref. [1] due to the failure to enforce certain initial conditions in the latter work. The peak force occurs early in the impact process, less than 100 μsec after impact, and the velocity curve starts at the correct initial value.

In this plastic impact case, the fitting procedure is not completely satisfactory in that the final projectile velocity cannot be established accurately due to lighting and camera limitations. Thus, the impulse–momentum law that represents one of the constraints of the data reduction process cannot be enforced exactly as is the case for the perforation runs, although the final results are quite satisfactory.

A comparison of the permanent deformation under static and transient load, shown in Fig. 6, indicates that the static profile is not nearly so localized, with significant deflections out to the clamped edge. The plastic energy absorbed in this case for a central loading of 700 lb was 152 in. lb which is slightly less than half of the 316 in. lb absorbed in run *AC*-3 that produced the same final central deflection of 0·52 in.

The permanent central deflection predicted by equation (7) is compared with experimental results in Fig. 21 and shows good correspondence for the assumed plate profile given by equation (6). A small correction has been used to account for the deviation from e^{-r} of the plate profile in the projectile contact area (see *A* in Fig. 6). The large amount of work-hardening present in 2024-0 aluminum requires its incorporation in the analysis,

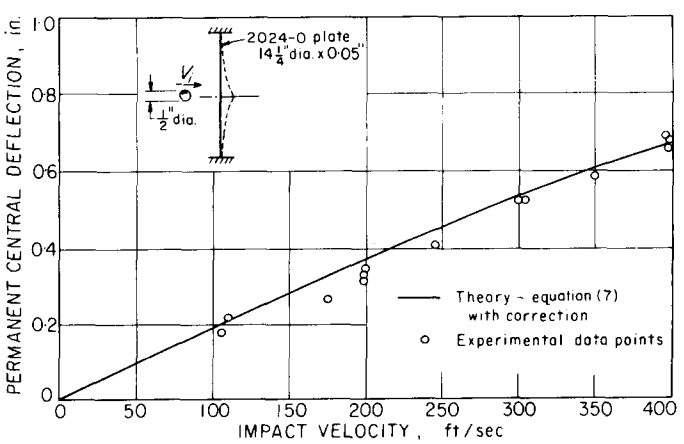

FIG. 21. Comparison of permanent deflection theory with experimental results for impact by a $\frac{1}{2}$ in. diameter steel sphere.

since strains of the order of 5 per cent or more are expected to exist in the region of impact. Stress–strain data for the plate materials showed that the stress level at 5 per cent strain is about 2·5 times the initial yield stress of 12,900 psi. As a number of simplifying assumptions have been used in the development of equation (7), it is possible that the good agreement with experiment could be due, in part, to a possible cancelling effect of these assumptions.

Perforation

Perforation of 2024-0 aluminum plates by spherical projectiles removes a cap, with dimensions given in Table 2, that has the shape of a segment of a spherical shell conforming to the surface of the striker. The top photograph in Fig. 17 clearly shows the effects of sphere perforation with some dishing and local plastic deformation apparent near the impact point.

The process of perforation of a thin aluminum plate by a $\frac{1}{2}$ in. diameter cylindro–conical projectile, illustrated in Fig. 13, shows eventual plate fracture along radial directions with an accompanying formation of petals. These radial fractures, as with the fractures of the plug for spherical projectiles, generally show a break at about 45° to the surface indicating a shearing type failure. An extension of V_i by a factor of over three relative to the previous study [1] is not sufficient to change the basic petalling mode of perforation.

Perforation by the $\frac{1}{2}$ in. sphere and the $\frac{1}{2}$ in. cylindro–conical projectile shows a general trend of decreasing momentum loss with increasing impact velocity. As would be expected, the loss in momentum and in kinetic energy for the sphere is considerably greater than that for the cylindro–conical projectile at the same initial velocity due to the much larger plastic deformation produced.

The radial strain histories for perforation by a sphere presented in Fig. 14 show a form similar to the plastic impact case, Fig. 3, except that peak strains decrease here with increasing projectile velocity. Though unloading disturbances apparently reach the 3 in. stations in runs *PC*-2 and *PC*-3 before the peak strain, the velocity of propagation of the peak strains also appears to be about 8800 in./sec, at least out to 3 in. from the point of impact. The peak strains at $r = 1\frac{1}{2}$ in. for the pointed projectile, Fig. 15, differ from previous results in being about the same for the three impact velocities even though the final permanent strain plateaus are not. However, the propagation velocity, assumed to be uniform between the $1\frac{1}{2}$ and 3 in. stations, is still about 8800 in./sec. The dynamic displacement history at the 2, 3, 4 and 5 in. stations for the two projectiles, shown for the sphere in Fig. 16, indicates essentially the same shape as that obtained for the plastic impact case. The dynamic plate profile shown in Fig. 18 is analogous to that depicting the formation and rising of a petal due to perforation by the cylindro–conical projectile [1].

The velocity drop data for the $\frac{1}{2}$ in. spherical projectile are compared with the theoretical result for a shear plug model, equation (9), in Fig. 22 for an assumed minimum perforation velocity V_x of 410 ft/sec. Though overpredicting ΔV, the curve does follow the same general trend as the data. The results for perforation by the $\frac{1}{2}$ in. conical projectile are shown in Fig. 23 with the experimental results of Ref. [1] included. In this case, equation (10) with a realistic value of $V_x = 240$ ft/sec, correlates well with the experimental data. However, the value of V_x is experimentally determined so the result is not purely analytical. The predictions of equation (8), and of equation (11), differ significantly from the data at low impact velocities but become more reasonable as the velocity is increased.

The complicated mechanism of perforation at low velocities requires a large number of simplifications for the construction of a suitable perforation theory resulting in a poor correspondence with experimental results, as was also found in Ref. [1]. This inability to adequately specify the motion of the plastic region near the point of impact leads to the failure of the various theories to describe the phenomena at low perforation velocities. As the impact velocity is increased, the extent of the plastic region decreases, and the theoretical results become more accurate.

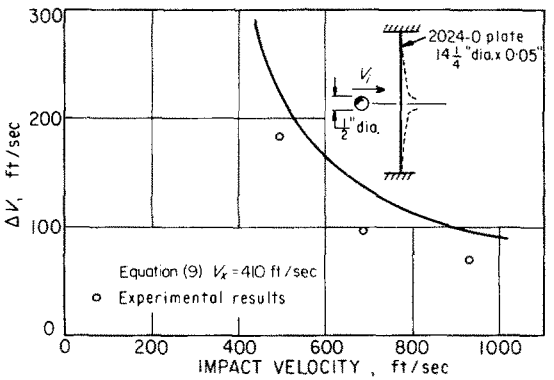

FIG. 22. Experimental velocity drop and comparison with theory for perforation by a $\frac{1}{2}$ in. diameter steel sphere.

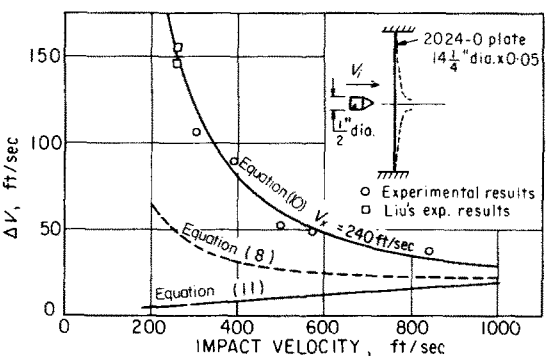

FIG. 23. Experimental velocity drop and comparison with theory for perforation by a $\frac{1}{2}$ in. diameter cylindro-conical steel projectile.

REFERENCES

[1] W. GOLDSMITH, T. W. LIU and S. CHULAY, Plate impact and perforation by projectiles. *Exp. Mech.* **5**, 385 (1965).
[2] H. G. HOPKINS and W. PRAGER, On the dynamics of plastic circular plates. *Z. angew. Math. Phys.* **5**, 317 (1954).
[3] A. L. FLORENCE, Clamped circular rigid–plastic plates under blast loading. *J. Appl. Mech.* **33**, 256 (1966).
[4] A. L. FLORENCE, Clamped circular rigid–plastic plates under central blast loading. *Int. J. Solids Struct.* **2**, 319 (1966).
[5] T. WIERZBICKI, Dynamics of rigid viscoplastic circular plates. *Archum Mech. Stosow*, **1**, 851 (1965).

[6] T. WIERZBICKI, Impulsive loading of rigid viscoplastic plates. *Int. J. Solids Struct.* **3**, 635 (1967).
[7] N. JONES, Impulsive loading of a simply supported circular rigid plastic plate. *J. Appl. Mech.* **35**, 59 (1968).
[8] D. E. BOYD, Dynamic deformations of circular membranes. *J. Engng Mech. Div. Am. Soc. Civ. Engrs* **92**, 1 (1966).
[9] H. G. HOPKINS, On the Impact Loading of Circular Plates Made of Ductile Metal, Div. App. Mech., Brown Univ. Report No. DA-2598/7, AD 22938 (1953).
[10] S. J. CHULAY, Dynamic Behavior of Plastic Plates, Ph.D. Dissertation, University of California (1966).
[11] J. M. KELLY and T. WIERZBICKI, Motion of a circular viscoplastic plate subjected to projectile impact. *Z. angew. Math. Phys.* **18**, 236 (1967).
[12] T. WIERZBICKI and J. M. KELLY, Finite deflection of a circular viscoplastic plate subject to projectile impact. *Int. J. Solids Struct.* **4**, 1081 (1968).
[13] J. M. KELLY and T. R. WILSHAW, A theoretical and experimental study of projectile impact on clamped circular plates. *Proc. R. Soc.* **306**, 435 (1968).
[14] M. ZAID and B. PAUL, Mechanics of high speed projectile perforation. *J. Franklin Inst.* **264**, 117 (1957).
[15] R. F. RECHT and T. W. IPSON, Ballistic perforation dynamics. *J. appl. Mech.* **30**, 384 (1963).
[16] T. A. DUFFEY, The Large Deflection Dynamic Response of Clamped Circular Plates Subjected to Explosive Loading, Sandia Corp. Res. Report No. SC-RR-67-532 (1967).
[17] H. A. BALMER, Improved Computer Programs—DEPROSS 1, 2, 3—To Calculate the Dynamic Elastic–Plastic Two Dimensional Responses of Impulsively Loaded Beams, Rings, Plates and Shells of Revolution, Mass. Inst. Tech., ASRL-TR 128-3 (1965).
[18] W. T. THOMSEN, An approximate theory of armor penetration. *J. appl. Phys.* **26**, 80 (1955).
[19] C. A. CALDER, Plastic Deformation and Perforation of Thin Plates Resulting from Projectile Impact, Ph.D. Thesis, University of California (1969).
[20] C. A. CALDER, A simple inexpensive projectile velocity gauge. *J. scient. Instrum.* **1**, 882 (1968).
[21] T. A. DUFFEY and S. W. KEY, Experimental–Theoretical Correlations of Impulsively Loaded Clamped Circular Plates, Sandia Corp. Res. Rep. No. SC-RR-68-210 (1968).
[22] A. L. FLORENCE, Circular plate under a uniformly distributed impulse. *Int. J. Solids Struct.* **2**, 37 (1966).
[23] G. MUNDAY and D. M. NEWITT, The deformation of transversely loaded discs under dynamic loads. *Phil. Trans. R. Soc.* **A256**, 1 (1963).

(*Received* 18 *February* 1970; *revised* 8 *June* 1970)

Абстракт—Исследуется экспериментально динамическое воздействие тонких пластинок, подверженных удару снаряда, путем иэмерения скорости снаряда, постоянной деформации, донамической деформации и перемещений, а также испытывая рост пластической деформации и движение снаряда с помощью быстродействующей кадровой камеры. Ьольшинство эсперимснтальной работы выполнено на полудюймых стальных снарядах, сфереческой или цилиндрическо—конической формы, попадающих центрически в пластинку иэ аллюминия 2024-0, толщины 0,050 дойма; пластинка защемлена по окружности диаметра 14 1/4 дюймов. Скорости снардов колебаются в пределах от 75 до 933 фут/сек. Эти скорости выбраны таким способом, чтобы получить значительные пластические деформации при низких скоростях и полный сквозной пробой при высших скоростях. Оказывается что граница пластической зоны по округе распространяется от топки удара со скоростью около 8800 дюйма/сек при всех скоростях удара. Упрощенное решение при больших прогибах, касающиеся остаточного центрального прогиба жестко—пластичкских пластинок с линейным упрочнением, указывает на надлежащую сходимость с данными и кореляцию между разными теориями пробоя. Оказывается что экспериментальные результаты являются лучшими при росте скорости снаряда.